Two golden times in two-step contagion models

Wonjun Choi,[1] Deokjae Lee,[1] J. Kertész,[2,3] and B. Kahng[1,*]

[1] *CCSS, CTP and Department of Physics and Astronomy, Seoul National University, Seoul 08826, Korea*
[2] *Center for Network Science, Central European University, Budapest, Hungary*
[3] *Department of Theoretical Physics, Budapest University of Technology and Economics, Budapest, Hungary*

(Dated: June 28, 2017)

The two-step contagion model is a simple toy model for understanding pandemic outbreaks that occur in the real world. The model takes into account that a susceptible person either gets immediately infected or weakened when getting into contact with an infectious one. As the number of weakened people increases, they eventually can become infected in a rapid cascading process and a pandemic outbreak occurs. The time required to reach such a pandemic outbreak allows for intervention and is often called golden time. Here we find that there exist two types of golden times in the two-step contagion model, which scale as $O(N^{1/3})$ and $O(N^{1/4})$ with the system size N on Erdős-Rényi networks. They are distinguished by the initial number of infected nodes, $o(N)$ and $O(N)$, respectively. These golden times are universal even in other models showing discontinuous transitions induced by cascading dynamics. We hope that understanding this size dependency of the golden time is useful for controlling pandemic outbreak.

PACS numbers: 89.75.Hc, 64.60.ah, 05.10.-a

I. INTRODUCTION

Epidemic spread of diseases and rumors and their control and containment have become a central issue in recent years as the real world becomes "smaller". It is a general observation that there is a slow phase in the spreading process before the sudden pandemic outbreak [1]. This slow period is called golden time as it allows for intervention, which is much more difficult after the disease becomes global. Modeling of epidemic spread with essential factors is necessary to control catastrophic outbreaks within this golden time. To this end, several epidemic models have been investigated on complex networks, for instance, the susceptible–infected–removed (SIR) model [2, 3] and the susceptible–infected–susceptible (SIS) model [4]. Analytical and numerical studies of those models revealed that a continuous phase transition occurs on Erdős-Rényi (ER) random networks [5]. Thus, abrupt pandemic outbreaks on a macroscopic scale, which often occur in the real world, cannot be reproduced using those models.

Considerable effort has been devoted recently to construct mathematical models that exhibit a discontinuous epidemic transition at a finite transition point on complex networks. A natural way is to appropriately extend the conventional SIR and SIS models. For instance, an extended SIR model includes more than one infected state of different pathogens that are cooperatively activated in contagion: A person who is suffering from the flu can be more easily infected by pneumonia. This model is referred to as a cooperative contagion model [6]. Similar instances include a two-step contagion process. A patient becomes weakened first and then becomes sick. This model is referred to as the susceptible–weakened–infected–removed (SWIR) model [7–14]. In another instance of modified SIR models, a network evolves by rewiring links at a certain rate during the spread of contagion [15]. The rewiring takes into account the mobility of humans. Then, epidemic spread can be accelerated as the rewiring rate is increased, which can lead to a discontinuous transition representing the pandemic outbreak.

When diseases spread, we need to keep susceptible people separate from infected patients or vaccinate the susceptible people before the diseases spread on a macroscopic level. A recent study [16] showed that for the SWIR model on ER networks, a system exhibits a long latent period (called a golden time) within which measures can be taken, beyond which the disease spreads explosively over the system at a macroscopic level. Estimating the golden time is important for the prevention of pandemic outbreaks. Moreover, it is necessary to get early-warning signals if a critical threshold is approached [17].

It was revealed [16] that when a disease starts spreading from a single node, the golden time n_c scales as $n_c(N) \sim N^{1/3}$. Here we reconsider this problem and represent the pattern of disease transmission using a nonlinear mapping. We show that the linear and nonlinear terms of the nonlinear mapping separately behave dynamically well. The linear term is responsible for one-step contagion without weakened states and the nonlinear term describes the two step contagion, which includes weakened state. Thus, the previous result of $N^{1/3}$ for the golden time is consistent with the characteristic size of the giant cluster generated in the SIR model, thus it has got verified within this new framework. Next, we consider another case, which is the main concern of this paper, in which an epidemic starts to spread from endemic multiple seeds of $O(N)$ on ER networks. In this case, fluctuations induced by stochastic process of disease

* bkahng@snu.ac.kr

transmission in the early time regime change the scaling of the golden time to $n_c(N) \sim N^{1/4}$. We estimate this scaling behavior using the saddle-node bifurcation theory [18] and discuss the underlying mechanism.

We also notice that while disease spreads across the system within those golden times, the population of weakened nodes is accumulated, which is a generic feature of the SWIR model. Without such a population, a pandemic outbreak cannot occur. Accordingly, we propose that the population of weakened nodes can serve as an indicator of the early-warning signal. If such population decreases with time in real world, a pandemic outbreak would not occur.

Finally, we show that the size dependence of the golden time is universal in other models showing discontinuous percolation transitions into an absorbing state induced by cascade dynamics [19], for instance, k-core percolation [20–23] and the threshold model [24, 25].

This paper is organized as follows: We first describe the SWIR model and set up the rate equation of the epidemic dynamics in Sec. II. Next, we derive a nonlinear mapping of epidemic spread in the SWIR model with a single seed in Sec. IIA. We show that the roles of the linear and nonlinear terms are well separated. In Sec. IIB, we derive a nonlinear mapping of epidemic spread for the case of multiple seeds and obtain the golden time. In Sec. III, we obtain the golden times for the multiple-seed case for k-core percolation and the threshold model and argue that the size dependence of the golden time is universal. A summary is presented in Sec. IV.

II. THE SWIR MODEL

The SWIR model is a generalization of the SIR model to include two states, a weakened state (denoted as W) and an infected state (I), between the susceptible state (S) and recovered state (R), instead of a single infected state I alone, as in the SIR model. Nodes in state W are involved in the reactions $S+I \to W+I$ and $W+I \to 2I$, which occur in addition to the reactions $S+I \to 2I$ and $I \to R$ in the SIR model. At each discrete time step n, the following processes are performed. (i) All the nodes in state I are listed in random order. (ii) The states of the neighbors of each node in the list are updated sequentially as follows: If a neighbor is in state S, it changes its state in one of two ways: either to I with probability κ or to W with probability μ. If a neighbor is in the state W, it changes to I with probability η, where κ, μ, and η are the contagion probabilities for the respective reactions. (iii) All nodes in the list change their states to R. This completes a single time step, and we repeat the above processes until the system reaches an absorbing state in which no infectious node is left in the system. The reactions are summarized as follows:

$$\mathrm{S} + \mathrm{I} \xrightarrow{\kappa} \mathrm{I} + \mathrm{I}, \tag{1}$$

$$\mathrm{S} + \mathrm{I} \xrightarrow{\mu} \mathrm{W} + \mathrm{I}, \tag{2}$$

$$\mathrm{W} + \mathrm{I} \xrightarrow{\eta} \mathrm{I} + \mathrm{I}, \tag{3}$$

$$\mathrm{I} \xrightarrow{1} \mathrm{R}. \tag{4}$$

In an absorbing state, each node is in one of three states, the susceptible, weakened, or recovered state. We define $P_S(\ell)$ as the conditional probability that a node remains in state S in the absorbing state, provided that it has ℓ neighbors in state R and was originally in state S. This means that the node remains in state S even though it has been in contact ℓ times with these ℓ neighbors in state I before they change their states to R. Thus, we obtain

$$P_S(\ell) = (1-\kappa-\mu)^\ell. \tag{5}$$

Next, $P_W(\ell)$ is similarly defined as the conditional probability that a randomly selected susceptible node is in state W after it contacts ℓ neighbors in state I before they change their states to R. The probability $P_W(\ell)$ is given as

$$P_W(\ell) = \sum_{n=0}^{\ell-1} (1-\kappa-\mu)^n \mu (1-\eta)^{\ell-n-1}. \tag{6}$$

Finally, $P_R(\ell)$ is the conditional probability that a node has been infected in any state, either I or R, provided that it was originally in state S and its ℓ neighbors are in state R in the absorbing state. Using the relation $P_S(\ell) + P_W(\ell) + P_R(\ell) = 1$, one can determine $P_R(\ell)$ in terms of P_S and P_W.

A. The single-seed case

First, we consider the case in which the number of infectious nodes is $o(N)$; that is, the density of initial seeds is $\rho_0 = 0$ in the thermodynamic limit. The order parameter m indicating whether a randomly chosen node is in state R after the system falls into an absorbing state is given using the local tree approximation as

$$m = \sum_{q=1}^{\infty} P_d(q) \sum_{\ell=1}^{q} \binom{q}{\ell} u^\ell (1-u)^{q-\ell} P_R(\ell), \tag{7}$$

where $P_d(q)$ is the probability that a node has degree q, and u is the probability that an arbitrarily chosen edge leads to a node in state R or I but not infected through the chosen edge in the absorbing state. In this case, the SWIR model exhibits a mixed-order transition [13] at a transition point κ_c when the mean degree is larger than a critical value. The order parameter displays a discontinuous transition from $m(\kappa_c) = 0$ to m_0, whereas other physical quantities such as the outbreak size distribution

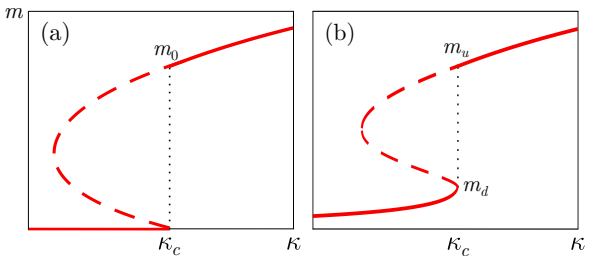

FIG. 1. Schematic plots of the order parameter $m(\kappa)$ versus κ for (a) $\rho_0 = 0$ (the single-seed case) and (b) $\rho_0 > 0$ (the multiple-seed case). (a) Even though κ is increased, the order parameter remains zero up to a transition point κ_c. However, at κ_c, it remains at $m = 0$ or jumps to m_0. For (b), as κ is increased, $m(\kappa)$ gradually increases from ρ_0 to a finite value m_d at κ_c. At κ_c, $m(\kappa)$ remains at m_d or jumps to m_u.

exhibit critical behavior. The behavior of the order parameter $m(\kappa)$ as a function of κ is schematically shown in Fig. 1(a).

We are interested in how infected nodes spread as a function of the cascade step n when the order parameter jumps. We define u_n similarly to u but at time step n. The probability u_{n+1} can be derived from u_n as follows:

$$u_{n+1} = \sum_{q=1}^{\infty} \frac{qP_d(q)}{z} \sum_{l=0}^{q-1} \binom{q-1}{\ell} u_n^{\ell}(1-u_n)^{q-1-\ell} P_R(\ell) \equiv f(u_n), \tag{8}$$

where the factor $qP_d(q)/z$ is the probability that a node connected to a randomly chosen edge has degree q. As a particular case, when the network is an ER network having a degree distribution that follows the Poisson distribution, i.e., $P_d(q) = z^q e^{-z}/q!$, where $z = \sum_q qP_d(q)$ is the mean degree, the function $f(u_n)$ is reduced as follows:

$$f(u_n) = 1 - \left(1 - \frac{\mu}{\kappa+\mu-\eta}\right) e^{-(\kappa+\mu)zu_n} - \frac{\mu}{\kappa+\mu-\eta} e^{-\eta z u_n}. \tag{9}$$

We remark that on ER networks, u_n in the limit $n \to \infty$ becomes equivalent to m obtained from Eq. (7).

We pick up the contribution of the reaction $S+I \to 2I$ from Eq. (9) but neglect the contribution of the reaction $W + I \to 2I$. Then, the probability that a node becomes directly infected by ℓ infectious neighbors, which is denoted by $P_R^{(S\to I)}(\ell)$, is given as

$$P_R^{(S\to I)}(\ell) = \sum_{m=0}^{\ell-1} (1-\kappa-\mu)^m \kappa = \frac{\kappa}{\kappa+\mu}[1-(1-\kappa-\mu)^{\ell}]. \tag{10}$$

Applying the formula for the Poisson degree distribution to Eq. (8), we obtain that

$$f^{(S\to I)}(u_n) = \frac{\kappa}{\kappa+\mu}\left[1 - e^{-(\kappa+\mu)zu_n}\right]. \tag{11}$$

Because the order parameter increases from $m = 0$, we assume that u_n is small in the early time regime. Thus,

$$u_{n+1}^{(S\to I)} = z\kappa u_n - a u_n^2 + O(u_n^3), \tag{12}$$

where $a \equiv \kappa(\kappa+\mu)z^2/2$. Actually, the coefficient $z\kappa$ of the first-order term is the mean branching ratio in the early time regime. When the critical branching (CB) process occurs, the mean branching ratio becomes unity, so the transition occurs at $\kappa_c = 1/z$. On the other hand, the discrete mapping (12) at κ_c may be rewritten in the form of a saddle-node bifurcation, $\dot{u}^{(S\to I)} = -au^2$, where u is a function of the continuous time variable n and the overdot denotes differentiation with respect to it. Because $a > 0$, $u^* = 0$ is a stable fixed point for $u \geq 0$, and this point represents the fixed point of the SIR model, indicating a second-order transition.

Next, we consider the two successive reactions $S+I \to W+I$ and $W+I \to 2I$, in which a susceptible node becomes infected in two steps and eventually recovers. Because a node can be infected either by the reaction $S+I \to 2I$ or by the reactions $S+I \to W+I$ and $W+I \to 2I$, the probability $f^{(S\to W\to I)}(u_n)$ can be obtained using the relation

$$f^{(S\to W\to I)}(u_n) = f(u_n) - f^{(S\to I)}(u_n) \tag{13}$$

as

$$f^{(S\to W\to I)}(u_n) = \frac{\mu}{\kappa+\mu}\left[1 + \frac{\eta}{\kappa+\mu-\eta} e^{-(\kappa+\mu)zu_n}\right] - \frac{\mu}{\kappa+\mu-\eta} e^{-\eta z u_n}. \tag{14}$$

Again, using $u_n \ll 1$, we obtain that

$$u_{n+1}^{(S\to W\to I)} = b u_n^2 + O(u_n^3), \tag{15}$$

where $b \equiv \mu\eta z^2/2$. Here we note that the first-order term $O(u_n)$ is absent. This discrete mapping is rewritten in the form of a transcritical bifurcation, $\dot{u} = -u + bu^2$. There exist one stable fixed point $u^* = 0$ and one unstable fixed point $u^* = 1/b$. For $0 < u < 1/b$, the dynamics flows into $u^* = 0$, whereas for $u > 1/b$, it flows out from $u^* = 1/b$. Combining Eqs. (12) and (15), we obtain that

$$u_{n+1} = u_n + (b-a)u_n^2 + O(u_n^3). \tag{16}$$

Thus, $\dot{u} = (b-a)u^2$. When $b-a < 0$, i.e., $\mu\eta < \kappa_c^2 + \kappa_c\mu$, the fixed point $u^* = 0$ is stable, and thus a continuous transition occurs. Otherwise, the fixed point $u^* = 0$ is unstable, and a discontinuous transition occurs. The condition $\mu\eta > \kappa_c^2 + \kappa_c\mu$ for a discontinuous transition is consistent with that previously obtained using the Landau–Ginzburg approach [7, 13].

When contagion starts from a single infectious node, its spread in the early time regime is governed by the linear term of Eq. (16). It proceeds in the form of a CB tree [16]. Specifically, when n is small (in the early time regime), the mean branching ratio $(u_{n+1} - u_n)/(u_n - u_{n-1})$ is almost unity, and the main contribution is that of the reaction $S + I \to 2I$. However, as time passes, the contribution of the nonlinear term $-au_n^2$ for the reaction $S + I \to 2I$ increases gradually, so the mean branching ratio decreases slowly. However, owing to the slow spread of CB process, the decrease is hardly noticeable

in the early time regime. This CB process is sustained for a long time until the contagion dynamics is perturbed by the finite-size effect. This behavior is shown in Fig. 2(a). On the other hand, the branching ratio of the two-step reaction for $S + I \to W + I$ and $W + I \to 2I$ becomes $(u_{n+1} - u_n)/(u_n - u_{n-1}) = 2bu_n$, which is almost zero in the early time regime because we start from $u_0 = 1/N$. However, u_n increases gradually, because $u = 0$ is an unstable fixed point and $b > 0$, as shown in Fig. 2(a). The growth rate of u for both the one-step and two-step reactions becomes $(b - a)u_n^2$ from Eq. (16). We find numerically that $a \approx 0.736$ and $b \approx 1.8$; thus, $b > a$ for the parameter values $\kappa = 1/8$, $\mu = 1/16$, and $\eta = 0.9$. Thus, supercritical epidemic spread is prevalent. Conclusively, in the early time regime, the one-step contagion dynamics is dominant, whereas in the late time regime, the two-step contagion dynamics leads to a pandemic outbreak, as shown in Fig. 2(a) and (b). For the mapping (16) with $b > a$, the role of the nonlinear term is quite distinct, leading to a discontinuous transition.

In the thermodynamic limit, u_n always stays zero so that nonlinear terms in Eq. (16) do not appear. On the other hand, in finite systems, u_n grows gradually and nonlinear term becomes significant after a characteristic time $n_c(N)$. On the other hand, it was argued in [26] that for the SIR model at the epidemic threshold, the maximum size of outbreaks is proportional to $N^{2/3}$ in the mean field limit. When u_n grows up to $O(N^{2/3})$, the nonlinear terms in Eq. (12) suppresses further growth of the cluster, leading to a subcritical branching process. This means that the CB process driven by Eq. (12) persists up to $O(N^{1/3})$, because the fractal dimension of the CB tree is two. On the other hand, for the SWIR model, the coefficient of the nonlinear term (16) is positive, and the nonlinear term encourages further increase of removed nodes. The CB process turns into a supercritical process, leading to a pandemic outbreak. Accordingly, the golden time, the duration of the CB process, scales similarly as $\sim N^{1/3}$ to that of the SIR model, which is what we observed in a previous work [16].

It may be interesting to notice that in the SWIR model, the population of weakened nodes increases with time step, whereas in the SIR model, such behavior cannot be found. Thus, the increasing pattern of the population of weakened node can be an indicator of a forthcoming pandemic outbreak.

B. The multiple-seed case

Next, when the number of infectious nodes is $O(N)$, i.e., the initial density of seeds is finite as $\rho_0 > 0$ in the thermodynamic limit, there exists a critical value $\rho_0^{(c)}$ such that when $\rho_0 < \rho_0^{(c)}$, a hybrid phase transition occurs [9–11, 14] at a transition point κ_c, whereas when $\rho_0 = \rho_0^{(c)}$, a continuous transition occurs. Here we focus on the formal case, in which the order parameter $m(\kappa)$ increases continuously as κ is increased from zero and exhibits critical behavior as κ approaches κ_c as shown in Fig. 1(b). Subsequently, the order parameter jumps from $m(\kappa_c) = m_d$ to another value m_u as represented in Fig. 1(b). Thus the transition is hybrid.

We notice that for the multiple-seed case, an infected node can be in contact with a node that was weakened by a different infectious root [14]. Accordingly, the reaction $W + I \to 2I$ can occur even in the early time regime, as shown in Fig. 2(c) with red zig-zag curve. Moreover, the CB process appears not from the beginning but slightly after that indicated by an arrow at n^* in Fig 2(c). We find that the density of recovered node r_{n^*} is close to m_d indicated in Fig. 1(b). From this step n^*, r_n almost remains for a long time as shown in Fig. 2(d). This means that r_n is trapped around m_d by the so-called bottle-neck effect as we discuss later. For some configurations, the dynamics is trapped at m_d forever, but for other configurations, it escapes from the trap and so the plateau ends at n_c, and then r_n increases abruptly and reaches a stable point m_u. We focus on the latter case in the following.

The recursive equation for u_n is written as

$$u_{n+1} = \rho_0 + (1 - \rho_0) f(u_n, \kappa), \tag{17}$$

where $f(u_n, \kappa)$ is equivalent to $f(u_n)$ in Eq. (9), but for further discussion, we explicitly present κ in the form of $f(u_n, \kappa)$. The epidemic dynamics begins at $n = 0$ with the densities of susceptible, weakened, infected and recovered nodes $s_0 = 1 - \rho_0$, $w_0 = 0$, $i_0 = \rho_0$ and $r_0 = 0$, respectively. Generally, the densities of each species of nodes at a certain time step m are denoted as s_m, w_m, i_m, and r_m, respectively. Then for $n > m$, $h_{n,m} \equiv u_n - r_m$ satisfies

$$h_{n+1,m} = i_m + s_m f(h_{n,m}) + w_m g(h_{n,m}) \tag{18}$$

where

$$\begin{aligned} g(h_{n,m}) &= 1 - \sum_{q=1}^{\infty} \frac{qP_d(q)}{z} \big[h_{n,m}(1 - \eta) + (1 - h_{n,m})\big]^{q-1} \\ &= 1 - e^{-\eta z h_{n,m}}, \end{aligned} \tag{19}$$

where the last step is valid for the ER case. With $r_0 = w_0 = 0$, $i_0 = \rho_0$, and $s_0 = (1 - \rho_0)$ at $m = 0$, Eq. (18) reduces to Eq. (17). Particularly, we denote $m_d - r_m$ as $h_{d,m}$, which becomes a fixed point of Eq. (18). When the epidemic dynamics starts from infected nodes with density ρ_0, then s_{n+1} (w_{n+1}) is determined by right hand side of Eq. (8) but $P_R(\ell)$ is replaced by $P_S(\ell)$ ($P_W(\ell)$). Thus, we can trace s_m and w_m at each time step m. Moreover, using Eq. (8) and the relation $i_n = u_{n+1} - u_n$, we can trace i_m and r_m as well.

In finite systems, fluctuations arise in those densities due to the randomness of infected nodes and stochastic process of epidemic spread. These fluctuations are there at the characteristic time n^*, from which the CB process begins. To take into account those fluctuations, we

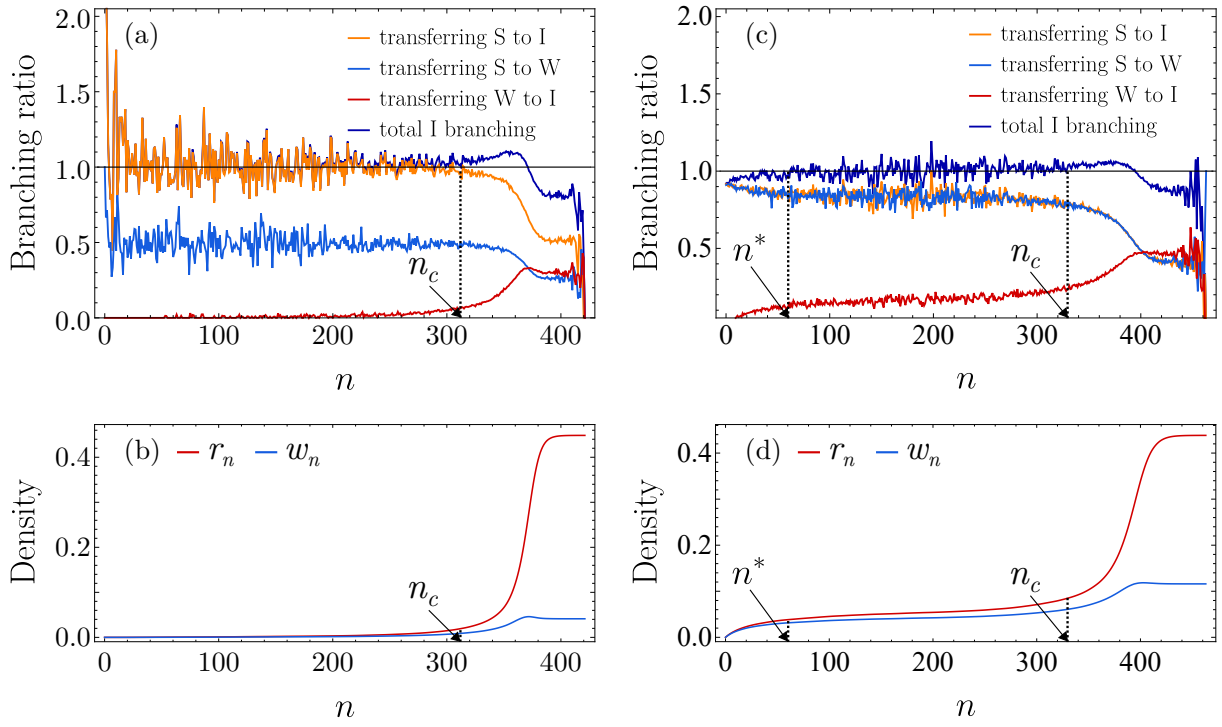

FIG. 2. (a) For the single-seed case, plot of the branching ratios as a function of time step n for each type of reaction at $\kappa_c = 1/8$. (b) Evolution of the densities of recovered nodes (red curve, top) and weakened nodes (blue curve, bottom) as a function of n for the single-seed case. Data are obtained from a single realization of infinite outbreak in the SWIR model starting from a single seed ($\rho_0 = 0$) with reaction probabilities $\mu = 1/16$ and $\eta = 0.9$ for both (a) and (b). (c) Similar to (a) but for the multiple-seed case at $\kappa_c \approx 0.1149487$. (d) Similar to (b) but for the multiple-seed case. For both (c) and (d), data are obtained using the parameters $\rho_0 = 0.002$, $\mu = \kappa$, and $\eta = 0.5$. The ER networks on which the simulations were performed have a size $N = 5.12 \times 10^6$ and mean degree $z = 8$. Legends "transferring X to Y" in (a) and (c) indicate the mean number of neighbors of an infected node that change their state from X to Y at step n. In (d), the characteristic time steps n^* and n_c, from and at which the CB process starts and ends, respectively, are marked.

split the densities of each species of nodes into two parts: $x_{n^*} + \delta x_{n^*}$, where the first term represents mean value at n^*, and x does s, w, i and r, respectively. Each δx_{n^*} follows the Gaussian distribution with the standard deviation proportional to $N^{-1/2}$. Then for $n > n^*$, Eq. (18) becomes

$$h_{n+1,n^*} = i_{n^*} + \delta i_{n^*} + (s_{n^*} + \delta s_{n^*}) f(h_{n,n^*}) + (w_{n^*} + \delta w_{n^*}) g(h_{n,n^*}). \quad (20)$$

At $\kappa = \kappa_c$, Eq. (20) is rewritten with $\epsilon_n = u_n - m_d$ as

$$\epsilon_{n+1} = d_1 + (1 + \delta d_2)\epsilon_n + (d_3 + \delta d_3)\epsilon_n^2 + O(\epsilon_n^3), \quad (21)$$

where

$$d_1 = \delta i_{n^*} \quad (22)$$

and

$$\delta d_2 = \delta s_{n^*} \frac{df}{dh}\bigg|_{h_{d,n^*}} + \delta w_{n^*} \frac{dg}{dh}\bigg|_{h_{d,n^*}} \quad (23)$$

$$d_3 = ((1-\rho_0)/2)(\partial^2 f(u_n, \kappa)/\partial^2 u_n)\big|_{m_d, \kappa_c} > 0 \quad (24)$$

$$\delta d_3 = \frac{1}{2}\left(\delta s_{n^*} \frac{d^2 f}{dh^2}\bigg|_{h_{d,n^*}} + \delta w_{n^*} \frac{d^2 g}{dh^2}\bigg|_{h_{d,n^*}} \right). \quad (25)$$

Eq. (21) is rewritten in an alternative form,

$$\dot{\epsilon} = d_1 + (d_3 + \delta d_3)\left(\epsilon + \frac{\delta d_2}{2(d_3 + \delta d_3)}\right)^2 - \frac{(\delta d_2)^2}{4(d_3 + \delta d_3)}. \quad (26)$$

Because $\delta i_{n^*} \sim \delta s_{n^*} \sim \delta w_{n^*} \ll 1$ for large N, the terms including δd_2 and δd_3 can be neglected compared with the respective leading terms and Eq.(26) is rewritten simply as

$$\dot{\epsilon} = d_1 + d_3 \epsilon^2 + O(\epsilon^3). \quad (27)$$

It is well known that the nonlinear mapping Eq.(27) includes the so-called bottleneck effect at $\epsilon = 0$ [18, 22, 27]. The time step to pass through the bottleneck is calculated as

$$\mathcal{T} = \int_{-\infty}^{\infty} \frac{d\epsilon}{d_1 + d_3 \epsilon^2} \sim \frac{\pi}{\sqrt{d_1}}, \quad (28)$$

which corresponds to the time interval of the plateau region, i.e, $n_c - n^*$. Because n^* is negligible to n_c, $n_c \sim \mathcal{T}$, which is the golden time for a single configuration.

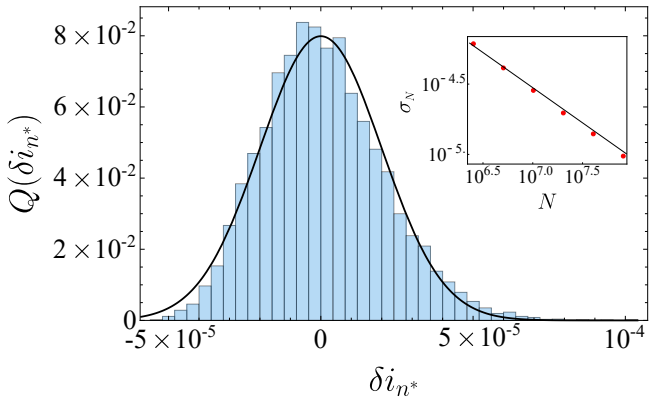

FIG. 3. The bar graph represents the numerical data of the distribution $Q(\delta i_{n^*})$ versus δi_{n^*} for a given system size $N = 2.048 \times 10^7$. The solid curve is a fitting to the Gaussian distribution. Inset: plot of estimated standard deviation of the Gaussian distribution versus the system size N. The solid line has a slope $-1/2$.

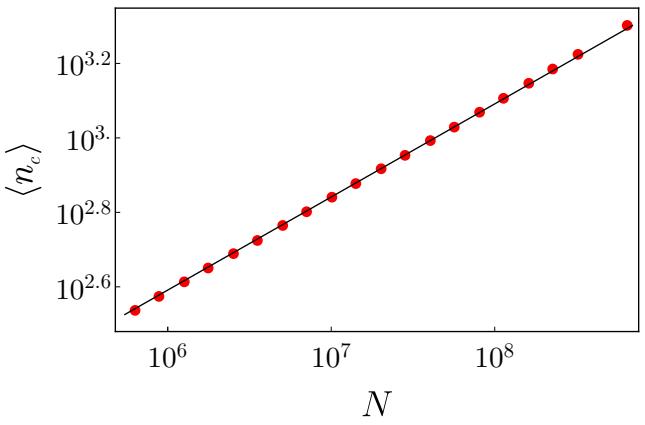

FIG. 4. For the multiple-seed case, plot of the average cascade time step $\langle n_c \rangle$ versus N at $\kappa_c \approx 0.1149487$. Guide line has a slope of 0.25. Data were obtained from ER networks of different sizes but with the same mean degree, $z = 8$. $\rho_0 = 0.002$, $\mu = \kappa$, and $\eta = 0.5$ were used.

Since $d_1 = \delta i_{n^*}$ follows the Gaussian distribution with the standard deviation proportional to $N^{-1/2}$, which was shown in Fig. 3, we introduce a probability distribution

$$Q(\delta i_{n^*}) = \frac{1}{\sqrt{2\pi\sigma_N{}^2}} e^{-\frac{(\delta i_{n^*})^2}{2\sigma_N{}^2}}, \tag{29}$$

where $\sigma_N \sim N^{-1/2}$. With Eq. (28) and Eq. (29) we obtain

$$\langle n_c \rangle \sim \int_0^\infty \frac{\pi Q(\delta i_{n^*})}{\sqrt{\delta i_{n^*}}} d(\delta i_{n^*}) \sim N^{1/4}. \tag{30}$$

This result is supported by Fig. 4. The integration is started from zero because no infinite outbreaks occur when $\delta i_{n^*} < 0$.

When $\kappa > \kappa_c$, d_1 is naturally obtained as $d_1 = (1 - \rho_0)(\partial f(u_n, \kappa)/\partial\kappa)\big|_{m_d,\kappa_c}(\kappa - \kappa_c)$. Thus, the golden time is determined. We do not need to take average over δi_{n^*} as

$$\langle n_c \rangle = \int_{-\infty}^{\infty} \frac{d\epsilon}{d_1 + d_3\epsilon^2} \sim \frac{\pi}{\sqrt{\kappa - \kappa_c}}. \tag{31}$$

Numerical result in Fig. 5 supports this prediction.

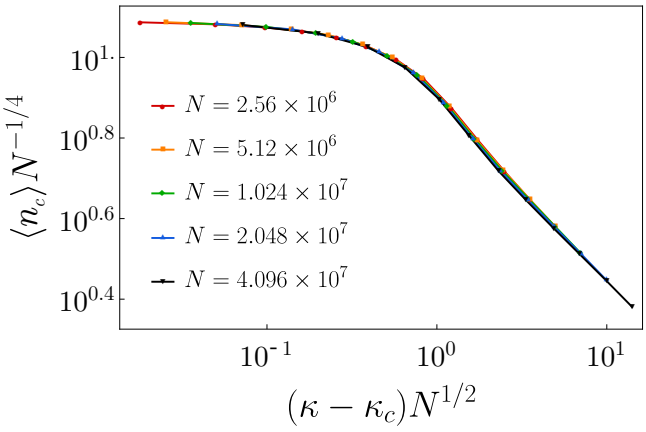

FIG. 5. For the multiple-seed case, scaling plot of the average cascade time step $\langle n_c \rangle N^{-1/4}$ versus $(\kappa - \kappa_c)N^{1/2}$ for different system sizes N. Data for different system sizes collapse well onto a single curve, indicating that $\langle n_c \rangle \sim N^{1/4}$ for $\kappa > \kappa_c$. Numerical simulations were performed on ER networks with mean degree $z = 8$ and initial density of seeds $\rho_0 = 0.002$.

III. UNIVERSAL BEHAVIOR

We also investigate the golden times of other models such as k-core percolation [20] and the threshold model [24]. We find that the golden time $\langle n_c \rangle \sim N^{1/4}$ is universal for epidemic disease spread initiated from multiple seeds.

A. k-core percolation

Here we first consider the avalanche dynamics of k-core percolation induced by failures of multiple nodes. In k-core percolation, the dynamics starts with the removal of all nodes that have degree less than k. These removals may decrease the degrees of the remaining nodes to less than k. If such nodes exist, they are removed as well. This process is repeated until no more such nodes remain. When the mean degree z of the original network is larger than a threshold z_c, a k-core subgraph of size $O(N)$ can exist. Next, we randomly remove a fraction ρ_0 of the remaining nodes and repeat the avalanche process. The avalanche size can be either finite or infinite depending

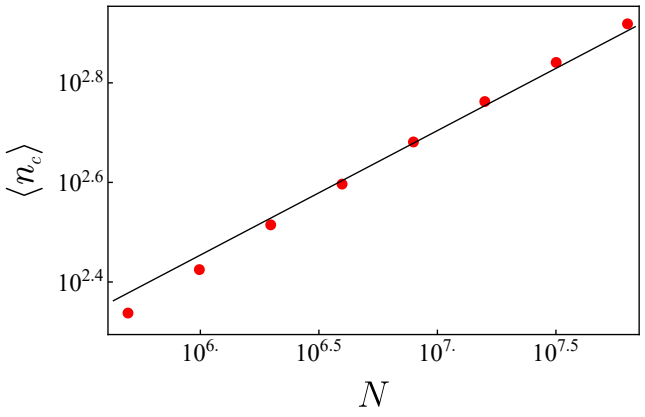

FIG. 6. Plot of the average cascade time step $\langle n_c \rangle$ versus N for k-core percolation with $k = 3$ starting from multiples nodes of $O(N)$. Guide line has a slope of 0.25. Data were obtained from ER networks of different sizes N but with the same mean degree, $z = 3.38476$, and $\rho_0 = 0.01$.

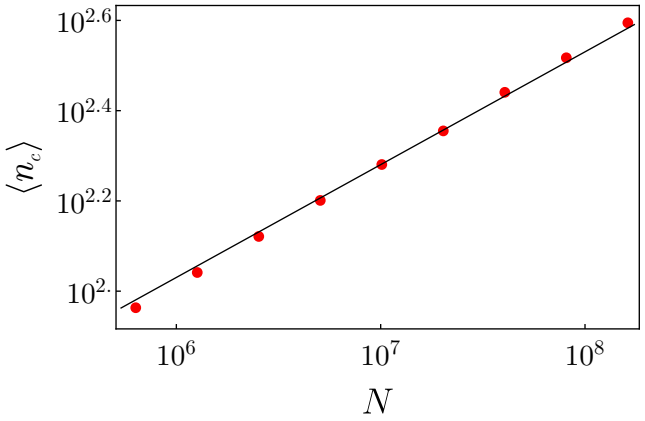

FIG. 7. Plot of the average cascade time step $\langle n_c \rangle$ for the threshold model starting from initial multiple active nodes. Guideline has a slope of 0.25. Data were obtained from ER networks of different sizes N but with the same $(z, \rho_0, \phi) = (9.191, 0.01, 0.18)$.

on z and ρ_0. If it is finite, the k-core would still exist; otherwise, it would collapse to zero. For sufficiently large z, there exists a critical density ρ_c such that an infinite avalanche can occur when $\rho_0 > \rho_c$ in the thermodynamic limit. In Fig. 6, we measure the mean cascade time step (golden time) $\langle n_c \rangle$ of infinite avalanches for different system sizes N. It was found that $\langle n_c \rangle \sim N^{0.28}$. The exponent is close to 1/4.

B. The threshold model

Next we consider the threshold model, which was introduced to study the spread of cultural fads on social networks. Each node i is assigned its threshold value ϕ_i and has one of two states, active or inactive. An inactive node i surrounded by m_i active neighbors and $k_i - m_i$ inactive neighbors changes its state to active when the fraction of active neighbors $m_i/k_i > \phi_i$. This threshold model is known to exhibit a hybrid phase transition on ER networks when the mean degree z is sufficiently large. Here, we initially introduce $\rho_0 N$ active nodes in a system. At each generation, every inactive node i whose number of active neighbors $m_i > k_i\phi_i$ is identified and changes its state to active. We performed simulations with a single threshold value $\phi_i = 0.18$ for all nodes on ER networks with $(z, \rho_0) = (9.191, 0.01)$. The mean cascade time step of infinite outbreaks, $\langle n_c \rangle$, is obtained as $\sim N^{0.263}$ in Fig. 7. The exponent is also close to 1/4.

IV. SUMMARY

The SWIR model is a simple model and enables us to understand pandemic outbreaks analytically. Using the local tree approximation at a transition point, we could represent the cascade dynamics of two-step contagion in terms of a nonlinear mapping that has the form of saddle-node bifurcation. When the epidemic dynamics starts from a single infected node, we showed that the linear and nonlinear terms of the nonlinear mapping have distinct roles. In the early time regime, the linear term governs a critical branching (CB) process of disease spread, which can be regarded as the growth of a cluster in percolation. However, in the late time regime, the nonlinear term causes explosive spread of epidemic disease. The golden time is determined by the finite-size effect on the linear term, which scales as $\sim N^{1/3}$. On the other hand, when the dynamics starts from multiple seeds of $O(N)$, the linear and nonlinear terms are coupled, and one cannot separate them. In this case, the golden time relies on the fluctuations induced by the stochastic process of disease transmission and the randomness of location of infected seeds. Those fluctuations lead to the so-called bottle-neck effect of the nonlinear mapping. Because such fluctuations are generated by random processes, the average bottle-neck size depends on the system as $\sim 1/\sqrt{N}$. Then, following the saddle-node bifurcation theory, the average golden time was obtained as $\sim N^{1/4}$, which was confirmed by numerical data. We also argued that the population of weakened nodes can play a role of an indicator of the forthcoming outbreak. Tracing the increasing or decreasing trend of this population is useful for predicting the pandemic. Furthermore, we showed that these two scaling behaviors are universal and can be obtained from other models showing discontinuous percolations into an absorbing state induced by cascade dynamics, such as k-core percolation and the threshold model.

ACKNOWLEDGMENTS

This work was supported by the National Research Foundation of Korea by grant no. NRF-2014R1A3A2069005 and by H2020 FETPROACT-GSS CIMPLEX Grant No. 641191 (JK).

[1] R. Pastor-Satorras, C. Castellano, P. Van Mieghem, and A. Vespignani, Rev. Mod. Phys. **87,** 925 (2015).
[2] D. Mollison, J. Royal Statist. Soc. **B 39,** 283 (1977).
[3] M. E. J. Newman, Phys. Rev. E **66,** 016128 (2002).
[4] R. M. Anderson and R. M. May, *Infectious Diseases in Humans* (Oxford University Press, Oxford, 1992).
[5] P. Erdős and A. Rényi, Publ. Math. **6,** 290 (1959).
[6] W. Cai, L. Chen, F. Ghanbarnejad, and P. Grassberger, Nat. Phys. **11,** 936 (2015).
[7] G. Bizhani, M. Paczuski, and P. Grassberger, Phys. Rev. E **86,** 011128 (2012).
[8] H.-K. Janssen, M. Müller, and O. Stenull, Phys. Rev. E **70,** 026114 (2004).
[9] H.-K. Janssen and O. Stenull, Europhys. Lett. **113,** 26005 (2016).
[10] T. Hasegawa and K. Nemoto, J. Stat. Mech. P11024 (2014).
[11] T. Hasegawa and K. Nemoto, arXiv:1611.02809.
[12] K. Chung, Y. Baek, M. Ha, and H. Jeong, Phys. Rev. E **93,** 052304 (2016).
[13] W. Choi, D. Lee, and B. Kahng, Phys. Rev. E **95,** 022304 (2017).
[14] W. Choi, D. Lee, and B. Kahng, Phys. Rev. E **95,** 062115 (2017).
[15] J. Yoo, J. S. Lee, and B. Kahng, Physica A **390,** 4571 (2011).
[16] D. Lee, W. Choi, J. Kertész, and B. Kahng, arXiv:1608.00776.
[17] M. Scheffer, et al., Nature **461**, 53 (2009).
[18] S. H. Strogatz, *Nonlinear Dynamics and Chaos* (Addison-Wesley, New York, 1994).
[19] D. Lee, S. Choi, M. Stippinger, J. Kertész, and B. Kahng, Phys. Rev. E **93,** 042109 (2016).
[20] J. Chalupa, P. L. Leath, and G. R. Reich, J. Phys. C **12,** L31–L35 (1979).
[21] S. N. Dorogovtsev, A. V. Goltsev, and J. F. F. Mendes, Phys. Rev. Lett. **96,** 040601 (2006).
[22] G. J. Baxter, S. N. Dorogovtsev, K. E. Lee, J. F. F. Mendes, and A. V. Goltsev, Phys. Rev. X **5,** 031017 (2015).
[23] D. Lee, M. Jo, and B. Kahng, Phys. Rev. E **94,** 062307 (2016).
[24] D. J. Watts, Proc. Natl. Acad. Sci. (U.S.A.) **99,** 5766 (2002).
[25] P. S. Dodds and D. J. Watts, Phys. Rev. Lett. **92,** 218701 (2004).
[26] E. Ben-Naim and P. L. Krapivsky, Phys. Rev. E **69**, 050901 (2004).
[27] S. V. Buldyrev, R. Parshani, G. Paul, H. E. Stanley, and S. Havlin, Nature **464,** 1025 (2010).